

Reduction of bandgap of ITO film and possibility of use as a window layer by incorporation of copper

M. Ahmed^a, A. Bakry^a, E. R. Shaaban^{b,*}, H. Dalir^c

^a*Department of Physics, Faculty of Science, King Abdulaziz University, 80203 Jeddah 21589, Saudi Arabia*

^b*Physics Department, Faculty of Science, Al - Azhar University, P.O. 71452, Assiut, Egypt*

^c*Department of Electrical and Computer Engineering, George Washington University, 20052, Washington, D.C., USA*

We report on reduction of the bandgap energy of ITO films by incorporation of copper along with thermal annealing for use as a window layer in optoelectronic applications such as solar cells. Using a conventional solid state reaction method, high purity In_2O_3 and SnO_2 (99.99%) powders were mixed in a mass ratio of 75:25 in a ball milling for about one hour to fabricate ITO alloys. Electron beam evaporation was used to prepare an ITO film with thickness of about 165 nm on a glass substrate. By immersing the films in a solution of $\text{Cu}(\text{NO}_3)_2$ (1g/1000ml) for 30 min, the prepared films were doped by ion exchange with Cu. Furthermore, the doped films were annealed in air at different temperatures for the diffusion of dopant Cu content (100, 150, 200, 250 and 300 °C) for 30 min. The (EDAX) was used to set the initial treatment composition. The XRD pattern was used to identify the cubic phase of the ITO films. Using spectroscopic ellipsometry, the film thickness, refractive index as well as extinction coefficient of the film was determined in terms of a three layers model. We show that the refractive index and extinction coefficient increase with incorporation of Cu and the annealing temperature. The possible transition in the as deposited and annealed films were found to allow direct transitions with reduction of the band gap energy from 3.50 to 2.75 eV with the increase of the annealing temperature. This means that the lower layer of ITO behaves as a window layer and is a shallow layer available as a buffer layer of solar cell.

(Received April 22, 2021; Accepted July 16, 2021)

Keywords: ITO:Cu films, EDAX, XRD, Spectroscopic ellipsometry, Optical constants, Energy gap

1. Introduction

Semiconductors of mixed oxides of In_2O_3 and SnO_2 have been playing an essential role concerning the special optical and electrical properties due to their wide band gap (3.062 –3.596 eV), high light transmittance, excellent electrical conductance, large flexible resistance and powerful chemical stability [1, 2]. Adding little amounts of SnO_2 to In_2O_3 can achieve the most useful outcome in terms of gas sensing and photocatalysis. ITO semiconductor materials also hold the interesting properties which qualify them to be utilized as active material in phased array systems for LiDAR applications in the IR and MID-IR, and in recent optoelectronic applications like solar cells, light emitting diodes, electrochromic windows, building curtain wall glass, plasma display panels (PDP), car windows, mirrors and lenses and other technological applications [3, 4]. ITO also hold considerable photo electrolytic properties that include electrical conductivity of 10^3 – $10^4 \text{ Ohm}^{-1}\text{cm}^{-1}$ and at the same time (90%) in the visible light region [5]. On the other hand, the electronic structure of the material is considerable to the effective performance. Though the lattice parameters of SnO_2 ($a = 4.594\text{Å}$, $c = 2.959\text{Å}$) are somewhat larger than those of In_2O_3 ($a = 4.737\text{Å}$, $c = 3.160\text{Å}$), via reaction between SnO_2 and TiO_2 at high temperature, a substitutional solid solution ITO with retained bottom redstone structure is obtained [6, 7]. Above 1450 °C, a solid solution with a composition range of $0.0 < x < 1.0$ is thermodynamically stable [8]. Lower than

* Corresponding author: esam_ramadan2005@yahoo.com

1450 °C, there is a nearly symmetric miscibility gap in which the solid solution decomposes spinodal into phases rich in Sn and In [9, 10]. However, such decomposition is very slow at room temperature, and rapid quenching of the composition near the end members ($x < 0.2$, $x > 0.8$) gives long-term stable single-phase samples [11]. Stable ITO can make the composition close to room temperature under kinetic control [12-16]. Moreover, the process of thermal annealing after-deposition of ITO films is an important method for the investigation to raise crystallinity and improve the electrical conductivity and optical transmission of films. Moreover, it can cause structural redress of ITO films and enhancement of carrier concentration that leads to a blue-shift of in energy gap [13, 17].

The target of this work is implantation of Cu into ITO thin films by the technique of ion exchange by immersing the prepared ITO films into a solution of $\text{Cu}(\text{NO}_3)_2$ for 30 min. These implanted films are annealed in vacuum to enhance diffusion of Cu into the films. The effects of annealing are studied on the optical constants (n , k) and optical band gap, E_g^{opt} of Cu implanted ITO films for solar cells applications. The optical studies are performed with high precision using spectroscopic ellipsometry in terms of a three layers optical model.

2. Experimental

Using the ball milling technology, high purity In_2O_3 and SnO_2 (99.99%) powders (purchased from Aldrich) were mixed in a mass ratio of 75:25 in a ball milling for about one hour to fabricate ITO alloys. The mixed powder is then pressed into disc-shaped pellets by a uniaxial compression (20 MPa), and then pressed at 210 MPa. Then the pellets were sintered at 1200 °C at a heating rate of 20 °C/min in 2-cap ambient atmosphere, and then cooled to space temperature at a rate of 20 °C/min. Such ITO particles are used as the initial material (after gridding), and the electron beam gun (Denton Vacuum DV 502 A) was used to deposit the powdered of ITO sample inside a quartz glass crucible at pressure of about 10^{-6} Pa onto clean glass substrates. FTM6 thickness monitor was used to monitor both the film thickness and rate of deposition. Through the fabrication process, the temperature of the substrate was set at 100 °C and the rate of deposition was at 2 nm/sec. ITO films were further submerged for 30 minutes with Cu doping in solution $\text{Cu}(\text{NO}_3)_2$ (1g/1000 ml). Then, these films were washed in distill water and dried out in compressing warmth air. In addition, for the diffusion of the dopant Cu material into ITO films, the heat treatment (annealing) was performed in vacuum at different annealing temperatures (100, 150, 200, 250 and 300 °C) for 30 min. X-ray diffraction (XRD) of powder (Philips diffraction 1710) was utilized to check the phase clarity and the structure of the ITO powder and films. The data of intensity were obtained using a small interval phase scanning mode ($\Delta 2\theta = 0.02^\circ$). Energy dispersive X-ray spectroscopy (EDAX) connected with a scanning electron microscope, SEM (JEOL JSM-6360LA, Japan), for composition analysis was used to confirm that the error of the indicator element unexceed 2.1%. A spectroscopic ellipsometry technique (J. A. Woollam Co., Inc.) was used for optical properties investigation.

3. Results and discussion

3.1. XRD and EDAX analysis

Rietveld refining is a method used to characterize crystalline materials [18]. The XRD pattern of the ITO powder sample is characterized by reflection (peak intensity) at convinced positions. The position, height and width of this reflection can be used to determine many aspects of the structure of the material. The Rietveld treatment utilizes the least squares method to treat the theoretical line contour until it matches the measured contour. Fig. 1 illustrates the sample grinding of Rietveld powder to ITO. Fig. 2 shows the diffraction peaks of the ITO films with different thicknesses in the XRD pattern belonging to the ITO (JCPDS data file: 39-1058-cubic), which is better oriented along the (222) plane. The main characteristics of these trends are the same, but only small differences are noticed during the peak duration. For the (222), (400), and

(411) orientation planes, the diffraction angles 2θ are 30.27, 35.17, and 50.98, respectively, and suitable sharp diffraction peaks are observed. Fig. 3 shows that as the film thickness grows, the diffraction intensity of the (222) plane increases, and the increase in thickness significantly improves the crystallization efficiency of the deposited film. Fig. 3(a) displays the stoichiometric composition of ITO in terms of EDXS. Also, the composition of implanted thick films of ITO:Cu were analysis using (EDXS) and the average value of Cu was about 9.55 at. % at almost the same in all treated films (Fig. 3 (b)).

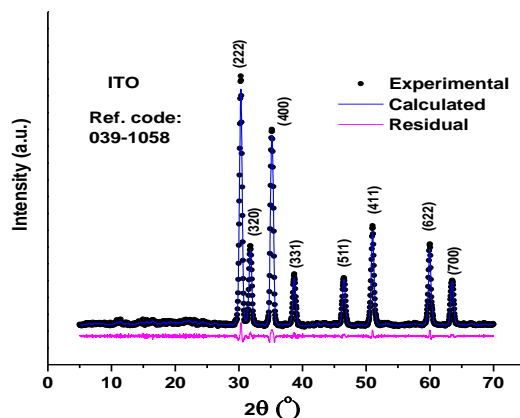


Fig. 1. XRD patterns and Rietveld refinement of polycrystalline ITO powder sample.

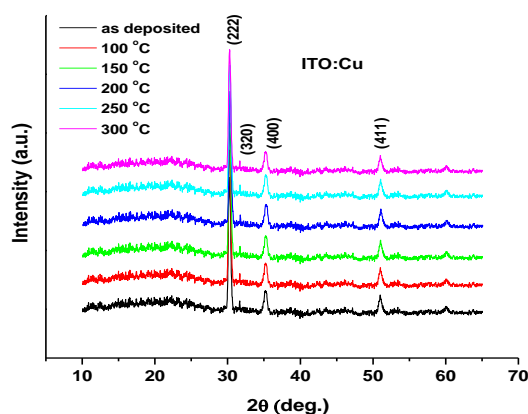


Fig. 2. XRD patterns of the ITO:Cu films as a function of different annealing temperature.

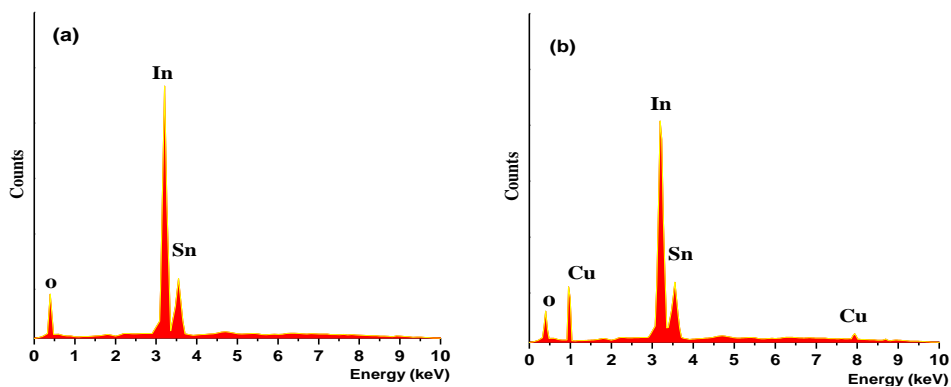


Fig. 3. EDXS spectra of (a) ITO film and (b) ITO:Cu film.

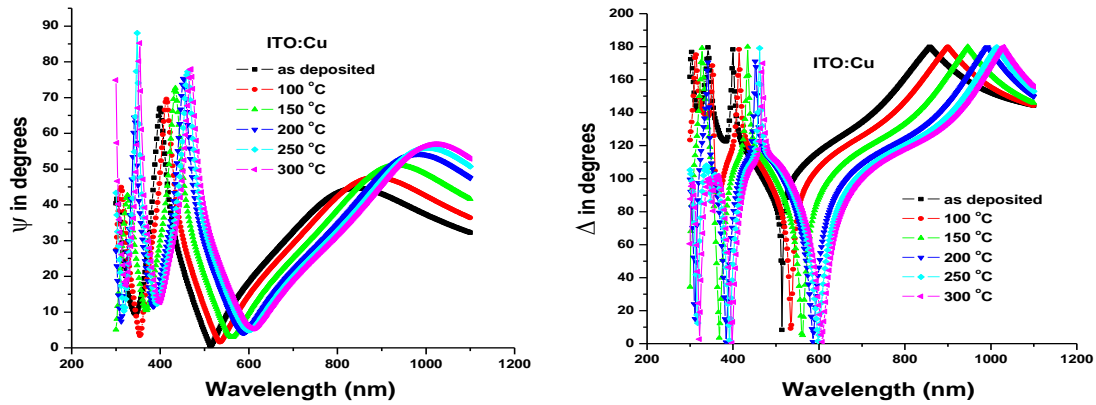


Fig. 4. The ellipsometric data versus wavelength ψ and Δ of ITO:Cu thin films with different annealing temperatures.

3.2. Calculation of optical constants of treated ITO:Cu using spectroscopic ellipsometry

The optical properties of ITO:Cu thin films at different annealing temperatures (100, 150, 200, 250 and 300 °C) are primarily studied by spectroscopic ellipsometry (SE), which measures the relative changes in amplitude and phase of the linearly polarized monochromatic incident light upon oblique reflection from the film surface. The appropriate experimental setups are required which determine non-redundant optical parameters from a general anisotropic sample. Generalized Ellipsometry (GE) comprises theory and experiment of anisotropy in layered samples. The experimental parameters obtained by standard SE (ψ and Δ) are related to the microstructure and optical properties as defined by [19]:

$$\rho = \frac{r_p}{r_s} = \tan \psi \exp(i \Delta) \quad (1)$$

Here r_s and r_p are the complex Fresnel's reflection coefficients of light polarized parallel (r_p) and perpendicular (r_s) to the plane of incidence, respectively. The layer model analysis, based on Fresnel's coefficients of reflection, is performed basing on the measured ellipsometric angles. The spectral dependencies of ψ and Δ were fitted in an appropriate model to extract the film thickness and optical constants; namely, refractive index (n) and extinction coefficient (k), using least square regression analysis and a weighted root mean square error function. The ellipsometric study applies a three layer models: upper layer (rough layer)/ absorbing ITO:Cu layer/ glass substrate. The upper layer that corresponds to the microscopic roughness obtained by SE is well correlated with the mean square error. The program is based on the least square regression to obtain the unknown fitting parameters and their maximum confidence limit. The procedure is to vary fitting parameters to minimize the differences between the measured and calculated ψ and Δ values. The Levenberg–Marquardt regression algorithm was used for minimizing the mean-squared error (MSE) [20]:

$$MSE = \frac{1}{2N-M} \sum_{i=1}^N \left(\left(\frac{\psi_i^{\text{mod}} - \psi_i^{\text{exp}}}{\sigma_{\psi,i}^{\text{exp}}} \right)^2 + \left(\frac{\Delta_i^{\text{mod}} - \Delta_i^{\text{exp}}}{\sigma_{\Delta,i}^{\text{exp}}} \right)^2 \right) \quad (2)$$

which has been used to judge the quality of the fit between the measured and the modeled data and is minimized in the fit. Here N is the number of measured ψ and Δ pairs included in the fit, M is

the number of fit parameters and i is the summation index. Also, ψ_i^{exp} , Δ_i^{exp} and ψ_i^{mod} , Δ_i^{mod} are the experimental and modeled values of ψ and Δ , respectively. $\sigma_{\psi,i}^{\text{exp}}$ and $\sigma_{\Delta,i}^{\text{exp}}$ are the experimental standard deviations in ψ and Δ respectively, which are calculated from the known error bars on the calibration parameters and the fluctuation of the measured data over averaged cycles of the rotating polarizer and analyzer. Eq. (3) has $2N$ and M in prefactor because there are two measured values included in the calculation for each ψ and Δ pair. The calculated data of ψ_i^{th} and Δ_i^{th} are generated by using the appropriate models as shown in Fig. Fig. 5 with corresponding dispersion relations [21]. The spectral dependencies of ψ and Δ determined for ITO:Cu films on glass substrate at different annealing temperature are depicted in Fig.4, respectively, the spectra show Fabry-Perot interference oscillations over the entire wavelength range originating from the multiple reflections within the films [22]. The SE parameters (ψ_i^{exp} , Δ_i^{exp}) for ITO films are demonstrated in Fig. 5, (red squares and blue dots) and the calculated data (ψ_i^{mod} , Δ_i^{mod}) plotted with black lines are presented. As clearly depicted in Figs. 5, good coincident between the measured SE parameters (ψ_i^{exp} , Δ_i^{exp}) and the calculated SE parameters (ψ_i^{mod} , Δ_i^{mod}) is achieved over the entire recorded wavelength regime. The MSE values generated by the harmony between measured and calculation SE parameters is 2.47. The estimated thicknesses for the surface roughness layer and for the ITO:Cu dense layer are shown in the inset of the Fig. 5 The estimated thicknesses of the films are about 165 ± 5 nm, respectively. The fitted optical constants, i.e. n and k of different thicknesses of ITO:Cu films are presented in Fig. 6 and Fig. 7, respectively. At any wavelength, the refractive index increases gradually with increasing the annealing temperature of ITO:Cu film. The refractive index (n) is closely related to the packing density of the films. Thus the increase in the refractive index may be attributed to the increase in the packing density with incorporation of Cu. Fig. 7 shows that at a shorter wavelength the value of the extinction coefficient (k) of ITO:Cu films arises with increasing the annealing temperature.

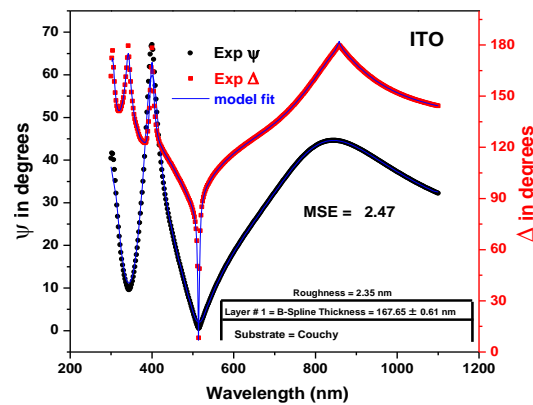


Fig. 5. SE data ψ_{exp} and Δ_{exp} (symbols) with fitting model (lines) of ITO films onto glass substrate.

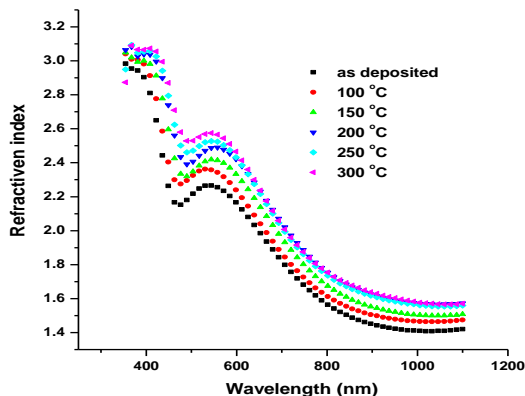


Fig. 6. The spectral variation of n determined from SE of ITO:Cu films onto glass substrate with different annealing temperatures.

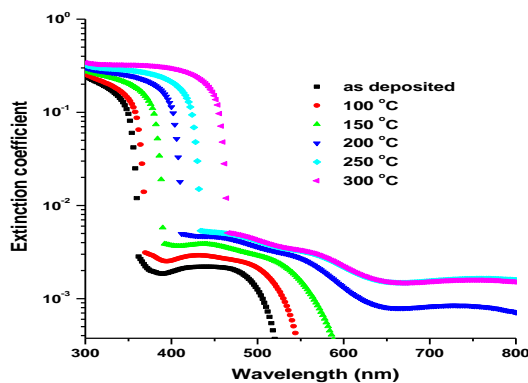


Fig. 7. The spectral variation of k determined from SE of ITO:Cu films onto glass substrate with different annealing temperatures.

The absorption coefficient ($\alpha h\nu$) of treated ITO:Cu thin films can be calculated from the values of the extinction coefficient k and λ using the known formula $k = \alpha\lambda/4\pi$. Fig. 8 illustrates dependence of the absorption coefficient $\alpha(h\nu)$ of the ITO:Cu thin films with different annealing temperature on the photon energy.

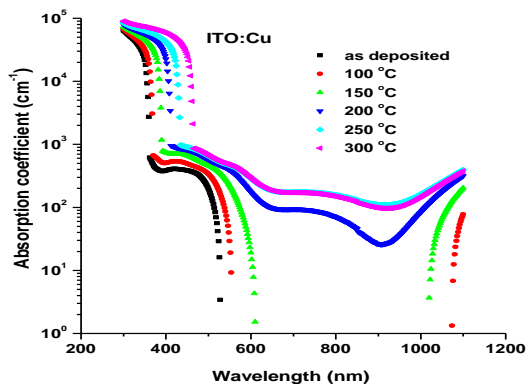


Fig. 8. Absorption coefficient versus photon energy of ITO:Cu films onto glass substrate with different annealing temperatures.

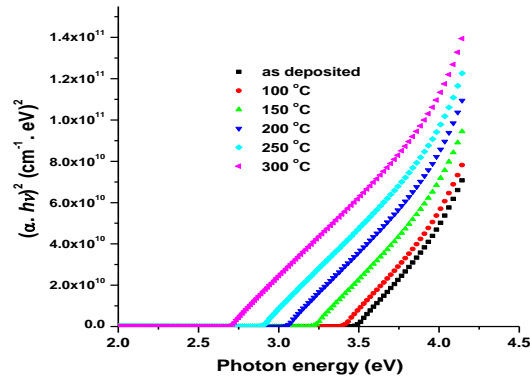


Fig. 9. $(\alpha h\nu)^2$ against $h\nu$ of ITO:Cu films at different annealing temperature.

It is known that in the vicinity of the fundamental absorption edge for allowed direct band-to-band transitions, the absorption coefficient is described by:

$$\alpha(h\nu) = \frac{K (h\nu - E_g^{opt})^m}{h\nu} \quad (3)$$

where K is a characteristic parameter (independent of photon energy) for respective transitions, $h\nu$ denotes photon energy, E_g^{opt} is optical bandgap energy and m is a number which characterizes the transition process. Different authors [23-25] have suggested different values of m for different glasses, $m=2$ for most amorphous semiconductors (indirect transition) and $m = 1/2$ for most of crystalline semiconductor (direct transition). In few reports, the band gap of SnS is classified as direct [26,27] and in other as indirect [28,29]. Therefore, the allowed direct and indirect optical bandgap energies of SnS films were evaluated from the $(\alpha h\nu)^2$ versus $h\nu$ and $(\alpha h\nu)^{1/2}$ versus $h\nu$ plots, respectively. Fig. 6 shows the $(\alpha h\nu)^2$ versus $h\nu$ plots of different annealing temperatures of ITO:Cu films. The $(\alpha h\nu)^2$ versus $h\nu$ plots of ITO:Cu films exhibit a straight line whose intercept with the energy axis (at $(\alpha h\nu)^2 = 0$) gives the direct bandgap energy. The variation of direct bandgap energy with the annealing temperature is shown in Fig. 10. The values of E_g^{opt} for both direct and indirect transitions are found to decrease with increasing the annealing temperature. The decreasing of E_g^{opt} from 3.5 eV to 2.75 recommends that the ITO window layer converts to a buffer layer due to incorporation of Cu into ITO film by heat treatment for applications in solar cells.

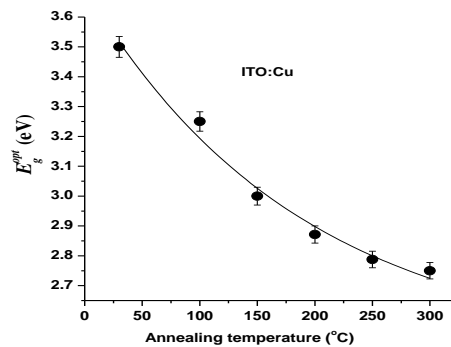


Fig. 10. Variation of direct bandgap energy with the annealing temperature

4. Conclusions

A conventional solid-state reaction method is used to mix high-purity In₂O₃ and SnO₂ powders at a mass ratio of 75:25 to manufacture an ITO alloy. The evaporated electron beam was used to prepare an ITO film with a thickness of about 165 nm on the glass substrate. In terms of ion exchange mechanism, the ITO film is doped with Cu. In order to diffuse the Cu material, the doped film is heat treated in air at different temperatures (100, 150, 200, 250 and 300 °C) for 30 minutes. The XRD spectra of the ITO: Cu film at different annealing temperatures show that there is no formation of a cubic structure of ITO with any other phase. The study of optical properties is carried out through spectral ellipsometry. Determine the film thickness and optical constants (n, k) were through a three-layer model: upper layer (rough layer)/absorptive ITO:Cu layer/glass substrate.

The upper layer corresponds to the microscopic roughness obtained by SE is well correlated with the mean square error. It is found that both n and k treated ITO:Cu films increase with the increase of annealing temperature. The results further show that as the annealing temperature increases from RT nm to 300 °C, the band gap with direct nature decreases. The conclusion is: as the annealing temperature increases, the optical constants of the ITO:Cu film increase. As the annealing temperature increases, the energy gap decreases from 3.5 eV to 2.75 eV. It means that the annealing improves the optical constant and energy gap of ITO:Cu, and it is recommended (ITO:Cu) to use it as a window as well as buffer layer for solar cells.

Acknowledgments

This project was funded by the Deanship of Scientific Research (DSR) at King Abdulaziz University, Jeddah, under grant no. (RG-38-130-41). The authors, therefore, acknowledge with thanks DSR technical and financial support. The authors would like to thank Prof. M. Abdel-Rahman at Minia University, Egypt for helpful discussion.

References

- [1] J. Wang, F. Luo, G. Ouyang, Y. Shi, *Physics Research Section B: Beam Interactions with Materials and Atoms* **450**, 234 (2019).
- [2] H. Koseoglu, F. Turkoglu, M. Kurt, M. D. Yaman, F. G. Akca, G. Aygun, L. Ozyuzer, *Vacuum* **120**, 8 (2015).
- [3] G. Li, C.-W. Chu, V. Shrotriya, J. Huang, Y. Yang, *Applied Physics Letters* **88**, 253503 (2006).
- [4] L. Zhao, Z. Zhou, H. Peng, R. Cui, *Applied surface science* **252**, 392 (2005).
- [5] B. Ren, X. Liu, M. Wang, Y. Xu, *Rare Metals* **25**, 137 (2006).
- [6] M. I Sayyed, Y Al-Hadeethi, M. M. AlShammari, M Ahmed, S.H. Al-Heniti, *Ceramics International* **47**, 611 (2021).
- [7] M. Emam-Ismail, M. El-Hagary, E. Shaaban, S. Moustafa, G. Gad, *Ceramics International* **45**, 8380 (2019).
- [8] L. Kong, J. Ma, H. Huang, , *Journal of alloys and compounds* **336**, 315 (2002).
- [9] Y Al-Hadeethi, M Ahmed, S. H. Al-Heniti, M. I. Sayyed, Y. S. Rammah, *Ceramics International* **46**, 19198 (2020).
- [10] M. Emam-Ismail, M. El-Hagary, E. R. Shaaban, A. M. Al-Hedeib, *Journal of alloys and compounds* **532**, 16 (2012).
- [11] E. R. Shaaban, Y. A. M. Ismail, H. S. Hassan, *Journal of non-crystalline solids* **376**, 61 (2013).
- [12] S. K. Kulshreshtha, R. Sasikala, V. Sudarsan, *Journal of Materials Chemistry* **11**, 930 (2001).
- [13] H. Guan, Y. Fang, X. Ma , *Chalcogenide Letters* **16** (9), 443 (2019).
- [14] M Ahmed, A Bakry, ER Shaaban, H Dalir, *Journal of Materials Science: Materials I Electronics* **32**, 11107 (2021).

- [15] C. Jin, I.-K. You, H.-K. Kim, , *Current Applied Physics* **13**, S177 (2013).
- [16] X. Song, M. Gao, Z. Huang, B. Han, Y. Wan, Q. Lei, Z. Ma, *Solar Energy* **173**, 456 (2018).
- [17] J.Kang, R. K. Kotnala, S. K. Tripathi , *Chalcogenide Letters* **17** (12), 631 (2020).
- [18] H. M. Rietveld, *J. Appl. Cryst.* **2**, 65 (1969).
- [19] H. Fujiwara, in: *Spectroscopic Ellipsometry: Principles and Applications*, Wiley, West Sussex, UK, 2007.
- [20] M Ahmed, A Bakry, A Qasem, H Dalir, *Optical Materials* **113**, 110866 (2021).
- [21] Y. Yamada, K. Tajima, M. Okada, S. Bao, M. Tazawa, K. Yoshimura, A. Roos, *Phys. Stat. Sol. C*, 1105 (2008).
- [22] E. R. Shaaban, I. S. Yahia, M. Fadel, *Journal of Alloys and Compounds* **469**, 427 (2009).
- [23] E. A. Davis, N. F. Mott, *Philos. Mag.* **22**, 903 (1970).
- [24] E. R. Shaaban, *Philosophical magazine* **88**, 781 (2008).
- [25] N. El-Kabnay, E. R. Shaaban, N Afify, A. M. Abou-Sehly *Physica B: Condensed Matter* **403**(1), 31 (2008).
- [26] M. Ichimura, K. Takeuchi, Y. Ono, E. Arai, *Thin Solid Films* **361–362**, 98 (2000).
- [27] N. Koteswara Reddy, K. T. Ramakrishna Reddy, *Thin Solid Films* **325**, 4 (1998).
- [28] M. Emam-Ismail, M. El-Hagary, E. R. Shaaban, S. Althoyaib, *Journal of alloys and compounds* **529**, 113 (2012).
- [29] A. Ortiz, J. C. Alonso, M. Garcia, J. Toriz, *Semicond. Sci. Technol.* **11**, 243 (1996).